SpheroidJ: A Generic Algorithm for Spheroid Segmentation

Anonymous ECCV submission

Paper ID

Abstract. Spheroids are the most widely used 3D models for studying the effects of different micro-environmental characteristics on tumour behaviour, and for testing different preclinical and clinical treatments. In order to speed up the study of spheroids, imaging methods that automatically segment and measure spheroids are instrumental; and, several approaches for automatic segmentation of spheroid images exist in the literature. However, those methods fail to generalise to a diversity of experimental conditions. In this work, we tackle this problem by developing a generic segmentation algorithm that can be easily adapted to different scenarios. The feasibility of applying our approach has been tested with several datasets of spheroid images where the spheroids were grown under several experimental conditions, and the images acquired using different equipment. In order to facilitate the dissemination and use of our method, we have implemented it in an open-source tool called SpheroidJ that has been released in the form of an ImageJ plugin and a standalone application.

Keywords: Spheroids; Segmentation; ImageJ; Java

1 Introduction

Cancer is the collective denomination for a group of diseases characterised by abnormal cell growth that can potentially disseminate, invade, and colonise different parts of the body. It is the second leading cause of death in the world, with approximately 9.6 million deaths per year [24]. A lot of important mechanisms of tumour progression have been described, which enabled development of treatments for various tumour types. However, the process of implementing one treatment in clinics is a long, expensive and complex process, as the treatment has to pass different proof stages. Namely, from tens of thousands of drugs tested, only one gets the approval for use [18]. This happens because most investigations have been done in two-dimensional (2D) cell culture, and on animal models. However, none of them represents well the human organism and its response to treatments. For example, 2D cultures fail to reproduce the complex structure of tumours and their interactions with the surrounding tissue, whereas animal models fail to fully mimic the in vivo situation of a human cancer patient. Hence, it is important to have a biomimetic preclinical model since such models may shorten preclinical trials and give more reliable results [1, 11]. Lately,

three-dimensional (3D) cell cultures are being developed to include cell-cell and cell-extracellular matrix interactions and all physico-chemical characteristics of microenvironment, as they have been described to play an important role in tumour progression and response to treatment [7].

Spheroids are the most widely used 3D models since they can be used for studying the effects of different micro-environmental characteristics on tumour behaviour and for testing different preclinical and clinical treatments. They are cellular aggregates that represent well cell-cell interactions, and formation of oxygen and nutrient gradients [13]. These induce the formation of necrotic core inside the spheroid, a common feature of solid tumours that is impossible to reproduce in 2D systems. Spheroids can be grown in suspension, replicating isolated solid tumour, or embedded in extracellular matrix proteins, simulating the invasive capacity of tumour cells. Both necrosis and invasion are indicators of tumour progression and prognosis and their inclusion in a 3D model is essential for obtaining a more accurate representation of an in vivo cancer.

However, since the interactions in 3D models are radically different from traditional 2D cultures, changes in imaging systems and analysing programs must be made to capture the new complexities. In particular, imaging methods that automatically segment and measure batches of spheroid images are instrumental for further analysis. Several software tools for spheroid segmentation are available in the literature in the form of ImageJ plugins [9,12], Matlab packages [3,8] or standalone programs [5, 15]. In addition, several commercial systems, like Celigo [23] or Phaedra [6]; or tools designed to work with concrete microscopes, such as ReViMS [16] and qVista [4], have been released. Due to the variance in sizes, shapes and textures of spheroids, all these tools are specialised in images acquired under certain conditions, and fail to generalise properly. An approach to deal with the generalisation problem is the application of data-based methods like deep learning [2, 20]; however, deep learning models for spheroid segmentation [22] are not freely available, and have not been tested in a diversity of experimental conditions.

In this paper, we approach the generalisation problem by developing a generic algorithm that can be easily adapted to different scenarios. Namely, the contributions of this work are threefold:

- First of all, we present a generic spheroid segmentation algorithm that can be particularised to different conditions, see Section 3.
- Subsequently, we conduct a thorough comparison of different variants of our generic algorithm with images of spheroids with different sizes, shapes and textures, see Section 4. We also compare our approach with several open-source tools, and show how well it generalises to different experimental conditions.
- Finally, we release our algorithm in the form of an ImageJ plugin and also as a user-friendly and standalone application called SpheroidJ, see Section 5.

2 Materials and methods

In our experiments, we have employed images from two different tumour spheroids under different experimental conditions. In addition, images were captured using different equipment (microscopes) and conditions (focus and magnification).

Human glioblastoma cell lines U87-MG and U251-MG and colorectal cancer cell line HCT-116 were purchased from Sigma Aldrich and American Type Culture Collection, respectively. All cell lines were cultured in high-glucose Dulbecco's modified Eagle's medium (DMEM) (Lonza, BE12-614F), supplemented with 10% foetal bovine serum (FBS) (Sigma, F7524), 1% L-glutamine (Lonza, 17-605C) and 1% penicillin/streptomycin (Lonza, 17-602E). In order to follow HCT-116 cells easier during a long period of time, they were transduced with a green fluorescent protein-expressing lentiviral vector, so while alive, cells produce fluorescent protein. All cell lines were grown in humidified incubator with 5% CO_2 and trypsinised twice a week.

Spheroids were formed using hanging drop method. Shortly, cells were harvested and resuspended at 40000 cells/mL in complete DMEM medium supplemented with 20% methocel. Drops of 25 μL were placed on the top of a petri dish and left for 48h for spheroid formation. For suspension culture, spheroids were transferred to round bottom 96 well plate (Sarstedt, 83.3925.500) treated with Anti-adherence rinsing solution (Stemcell, 07010). To investigate the importance of nutrients or growth factors present in microenvironment, spheroids were grown in media with different chemical composition. Besides, suspension culture was used to evaluate the efficacy of tested drugs. For invasion assays, spheroids were embedded in rat tail type I collagen hydrogels. Different final concentrations of collagen enabled studying the effect of different matrix stiffness on spheroid behaviour.

Spheroid growth and invasion were followed for up to two months by brightfield and fluorescence imaging, using Nikon Eclipse Ti-E C1 and Leica DMi8 microscopes. Transduced cells were imaged using GFP filter set. Images were acquired using 2x and 10x magnification on Nikon microscope and 5x on Leica microscope. The images were organised in 6 datasets (3 brightfield datasets and 3 fluorescence datasets), and their features are summarised in Table 1. In addition to those datasets, we have also employed the dataset provided in [9]. A sample from each dataset is provided in Figure 1.

3 Segmentation algorithms

In this section, we present our generic algorithm for segmenting spheroids. Such an algorithm can be particularised in different ways to produce distinct segmentation procedures that are useful for several scenarios.

3.1 Generic segmentation algorithm

Given an image containing a spheroid, our generic algorithm aims to produce a mask for the region that contains it. Our algorithm, that is diagrammatically

Table 1. Features of the 7 datasets employed in this work. The datasets are named with the following convention: the first character of the name indicates whether is a brightfield (B) or a fluorescence dataset (F); the second, the microscope; the third, the magnification; and, the fourth, the culture media.

Dataset	Method	♯ Images	Image size	Microscope	Magnification	Format	Type	Culture
BL5S	Brightfield	50	1296× 966	Leica	5x	TIFF	RGB	Suspension
BN2S	Brightfield	154	1002× 1004	Nikon	2x	ND2	Gray 16bits	Suspension
BN10S	Brightfield	105	1002× 1004	Nikon	10x	ND2	Gray 16bits	Suspension
FL5C	Fluorescence	19	1296× 966	Leica	5x	TIFF	RGB	Collagen
FL5S	Fluorescence	50	1296× 966	Leica	5x	TIFF	RGB	Suspension
FN2S	Fluorescence	34	1002× 1004	Nikon	2x	ND2	Gray 16bits	Suspension
BO10S [9]	Brightfield	64	3136 × 2152	Olympus	10x	JPG	RGB	Suspension

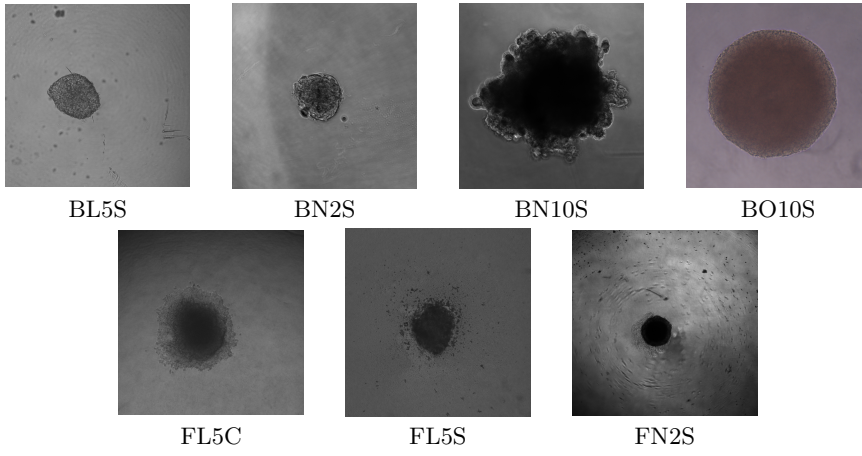

Fig. 1. Samples from the 7 datasets employed in this work

described in Figure 2, is based on the sequential application of several image processing techniques, such as edge detection or thresholding, and morphological operations like dilation or erosion. Namely, the procedure can be split into two steps: contour generation and contour refinement.

In the first step, the algorithm tries to find the contour of the spheroid, either by binarising the image, or by finding the edges of the image and later binarising it. This step can be particularised in two different ways. First, the Sobel edge detector [10] can be iterated several times on the image to detect a closed contour, this iterative procedure can be employed when the edges of the spheroid are not clear. And, second, the threshold values to binarise the image can be fixed manually, or automatically selected by using algorithms like IsoData [17] or Otsu [14].

Once the contour of the image is generated, the second step of our algorithm refines such a contour. First of all, the algorithm tries to close the contour region by applying several times the dilation operation, and subsequently filling the

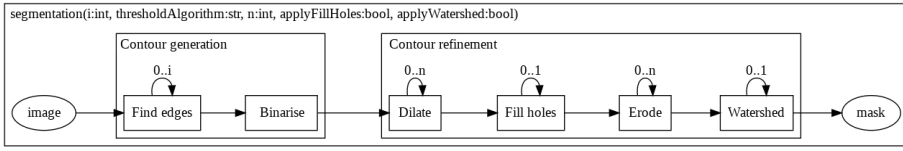

Fig. 2. Generic algorithm for spheroid segmentation

holes produced in the image. After applying the dilation operation, the contour region is bigger than the actual spheroid region; therefore, an erosion operation is applied to adjust that region. Finally, the watershed operation [19] is applied to remove artefacts that do not belong to the spheroid. An example showing the application of our procedure is depicted in Figure 3.

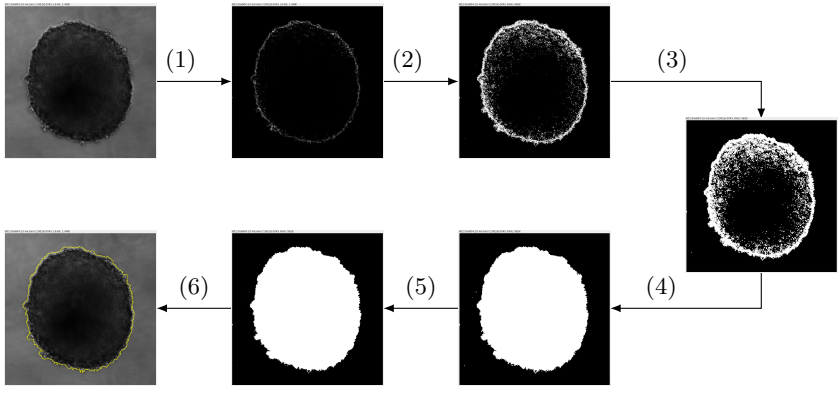

Fig. 3. Example of the application of our generic algorithm for a sample from the BN10S dataset. (1) Find edges; (2) Binarising; (3) Dilation; (4) Fill holes; (5) Erosion; (6) Final segmentation (in yellow)

As it can be noted from the above description, our generic algorithm can be customised by fixing 5 parameters: (1) the number of iterations that the Sobel edge detector is applied; (2) the thresholding method; (3) the number of times that the dilation and erosion operations are employed; (4) whether the fill holes operation is applied; and (5) whether the watershed operation is employed.

3.2 Particular algorithms

Due to the different nature of spheroid images, we have particularised our generic algorithm using 5 strategies; that is, using different values for the 5 parameters of our segmentation algorithm. In addition, several variants of our algorithm are combined to deal with those cases where a proper spheroid mask is not

generated. We consider a mask as valid when it has a minimum size and satisfies some solidity conditions — note that these conditions depend on the particular characteristics of the spheroid image. The rest of this section is devoted to present the 5 versions of our algorithm.

A1. Threshold. The first strategy is based on just binarising the spheroid images by using the IsoData method [17]. In those cases where such a direct approach does not produce a valid mask, we sequentially binarise the image, dilate it, fill the holes, erode the image, and, finally, apply the watershed operation. This straightforward approach is useful when the spheroid image can be clearly distinguished from the background of the image.

A2. Edges. The second strategy does not directly binarise the image but it firstly finds the edges of the image, and subsequently binarise the image using the IsoData method. In case that the method does not work, the number of iterations that the find edges operation is applied is increased. The process stops after a valid mask is found or when a number of iterations is reached.

A3. Threshold+Edges. This approach is a sequential application of Algorithms A1 and A2. Namely, it starts applying the threshold approach, and if it fails to find a valid mask, it applies the edges approach.

A4. Threshold & edges. This strategy applies both Algorithms A1 and A2 to the input image, adds the two resulting masks, and fills the holes of the resulting mask to produce the final output.

A5. Fluorescence. Finally, we have designed an algorithm that takes advantage of images acquired with fluorescence. To this aim, the normal image is processed by sequentially finding its edges and binarising it; and, the fluorescence image is binarised using the IsoData thresholding method. The two images produced in this way are combined using the AND binary operation to output the mask.

4 Results

In this section, we compare the different versions of our generic algorithm for the datasets presented in Section 2. In addition, we include in the comparison two open-source Fiji macros: Insidia [12], and the macro presented in [9] (from now on, this macro will be called "Ivanov"). The metric employed to measure the accuracy of the different methods is the IoU, also known as Jaccard index — this metric measures the area of intersection between the ground truth and the predicted region over the area of union between the ground truth and the predicted region — the ground truth was manually generated by experts using the free-hand tool of ImageJ [21]. We first analyse the 4 brightfield datasets; and, after that, the fluorescence datasets.

The results for the brightfield datasets are presented in Table 2. A statistical analysis of such results is also included. In particular, Friedman tests were carried

Table 2. Mean (and standard deviation) for the brightfield datasets. The best result for each dataset is highlighted in bold face, $^{***}\rho < 0.001$, > significant difference between methods. In and Iv stand for Insidia and Ivanov, respectively.

	Insidia	Ivanov	A1	A2	A3	A4	Friedman Test	Dunn test
BL5S	0(0)	0(0)	0.55(0.33)	0.31(0.42)	**0.63(0.39)**	0(0)	154.756^{***}	A3>A1>A2,A4,In,Iv
BN2S	0.65(0.35)	0.2(0.36)	0.93(0.04)	**0.94(0.02)**	0.72(0.35)	0.73(0.35)	427.632^{***}	A2,A1>A4>A3>In>Iv
BN10S	0.84(0.07)	0.03(0.18)	0.65(0.38)	0.69(0.42)	0.6(0.42)	**0.95(0.01)**	190.462^{***}	A4>In>A2,A1>A3>Iv
BO10S	0.91(0.09)	0.94(0.17)	**0.94(0.03)**	0.42(0.42)	0.79(0.36)	0.88(0.10)	224.473^{***}	A1,Iv>In,A4,A3>A2
Combined	0.64(0.37)	0.28(0.43)	**0.81(0.27)**	0.68(0.41)	0.7(0.39)	0.74(0.35)	385.751^{***}	A1>A4,A3,A2>In,Iv

out to compare the total scores for the six methods. When significant differences among the methods were found, a Dunn-Bonferroni pairwise post hoc test was also included. We can notice that there is not a single method that excels the others in all the datasets; but, our generic algorithm can be successfully adapted to several experimental conditions. In addition, our method outperforms both Insidia and Ivanov macros in most datasets.

On the contrary to the brightfield datasets, there is a method, Algorithm A5, that produces better results than the other algorithms for all the fluorescence datasets, see Table 3. This is due to the fact that, Algorithm A5, as well as humans, not only uses the brightfield image for segmentation, but it also takes advantage of the fluorescence image where the location of the spheroid region is clearly defined — the accuracy of all the other studied methods and macros is considerably lower than the accuracy obtained by Algorithm A5 since they only consider the brightfield image. However, since the spheroid region of a fluorescence image does not perfectly adjust to the spheroid, this produces a lower accuracy than the methods for the brightfield datasets.

Table 3. Mean (and standard deviation) for the fluorescence datasets. The best result for each dataset is highlighted in bold face, $^{***}\rho < 0.001$, > significant difference between methods. In and Iv stand for Insidia and Ivanov, respectively.

	Insidia	Ivanov	A1	A2	A3	A4	A5	Friedman Test	Dunn test
FL5C	0.12(0.24)	0.09(0.28)	0.53(0.37)	0(0)	0.4(0.37)	0(0)	**0.67(0.17)**	74.530^{***}	A5,A1,A3>In,Iv,A2,A4
FL5S	0.51(0.24)	0.04(0.1)	0.31(0.21)	0.04(0.14)	0.42(0.27)	0(0)	**0.89(0.07)**	191.062^{***}	A5>In,A3,A1>A2,Iv,A4
FN2S	0.03(0.02)	0(0)	0.65(0.3)	0.47(0.36)	0.02(0.16)	0.05(0.04)	**0.82(0.17)**	148.081^{***}	A5>A1,A2>A4,In,A3,Iv
Combined	0.25(0.29)	0.03(0.15)	0.48(0.32)	0.19(0.32)	0.27(0.32)	0.03(0.10)	**0.82(0.16)**	278.983^{***}	A5>A1,In,A3>A2,A4,Iv

As we have seen throughout this section, there is not a single method that always produce the best results for different datasets of spheroid images; and, therefore, it is worth trying different approaches. To facilitate the use and comparison of different methods, we have developed a tool called SpheroidJ.

5 SpheroidJ

We have released our generic algorithm in an open-source and freely available program, called SpheroidJ, that can be employed both as an ImageJ plugin, and also as a standalone application.

ImageJ [21] is an image-analysis tool that has been widely employed to deal with many problems in life sciences, and that can be easily extended by means of plugins. The SpheroidJ plugin can be called from the ImageJ interface and provides two executions modes: the batch mode and the experimental mode. The former allows the users to employ any of the 5 algorithms presented in Section 3.2 in a folder containing spheroid images. The latter allows the users to configure the generic algorithm presented in Section 3.1 to deal with their own images. The parameters of the algorithm can be configured from the window presented in Figure 4 and applied either to a single image or a folder of images. The result outputted by both modes are the spheroid segmentations, either of the given image or for each image of the given folder, and an Excel file with a summary of measures (such as the area, perimeter, circularity or Feret's diameter) extracted from the segmented images.

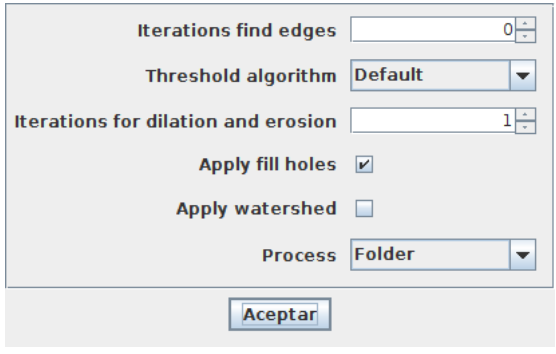

Fig. 4. SpheroidJ plugin window to configure the segmentation algorithm

This ImageJ plugin has a main drawback: it does not provide a simple way of visualising and editing the segmentation results when dealing with a folder of images. This issue has been tackled with the development of a user-friendly and standalone application. This tool provides the same functionality explained for the ImageJ plugin, but after the segmentation process, it shows the results using the interface presented in Figure 5. In this way, the users can easily inspect the segmentation result, try different algorithms for a single image, and manually edit the segmented region if it was not properly detected.

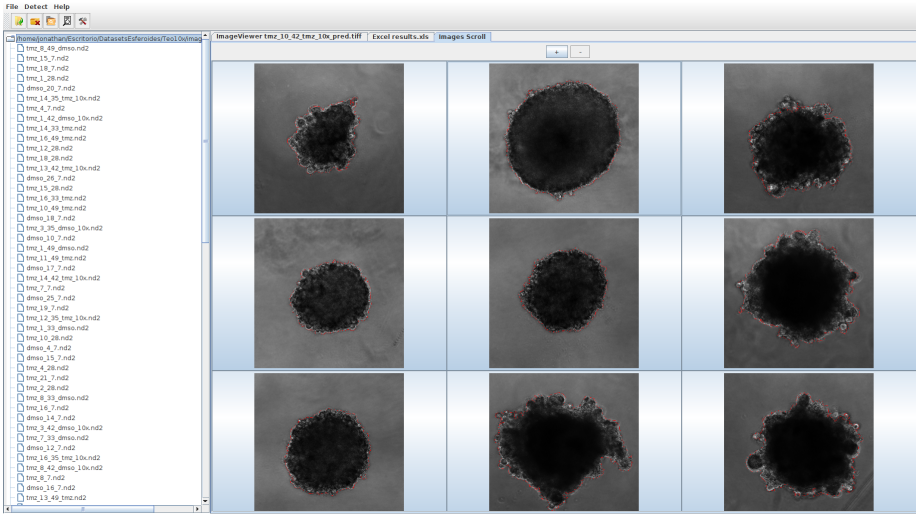

Fig. 5. SpheroidJ standalone application

6 Conclusions and further work

Due to the variance in sizes, shapes and textures of spheroids, it does not exist a single algorithm that generalises correctly to all the possible scenarios. In this paper, we have tackled this challenge by designing a customisable algorithm that can be successfully adapted to different kinds of spheroid images. In order to facilitate the dissemination of our method, we have released both an ImageJ plugin and a standalone application.

The main task that remains as further work is the development of a segmentation algorithm that works properly for images acquired under different conditions and using different equipment, and that does not require the configuration of several parameters. The most promising research line in this direction is the construction of deep learning segmentation models; however, there is a wide variety of segmentation algorithms; hence, a thorough study will be necessary.

Availability and requirements

SpheroidJ will be made freely available after the revision process. The ImageJ version of SpheroidJ can be installed from the ImageJ updater by adding the SpheroidJ site. The standalone tool can be installed from the project webpage. The datasets and ground truth employed in this work are also available at the project webpage.

References

1. Andrade, E.L., Benito, A., Cavalli, J., et al.: Non-clinical studies required for new drug development – Part I: Early in silico and in vitro studies,new target discovery and validation,proof of principles and robustness of animal studies. Brazilian Journal of Medical and Biological Research **19**(11), e5644 (2016). https://doi.org/10.1590/1414-431X20165644
2. Chen, L.C., Papandreou, G., Schroff, F., et al.: Rethinking atrous convolution for semantic image segmentation. ArXiv **abs/1706.05587** (2017)
3. Chen, W., Wong, C., Vosburgh, E., et al.: High-throughput image analysis of tumor spheroids: A user-friendly software application to measure the size of spheroids automatically and accurately. Journal of Visualized Experiments **89**, e51639 (2014). https://doi.org/10.3791/51639
4. Cisneros-Castillo, L.R., Oancea, A.D., Stüllen, C., et al.: An imaging-based platform for high-content, quantitative evaluation of therapeutic response in 3d tumour models. Scientific Reports **4**, 3751 (2015). https://doi.org/10.1038/srep03751
5. Cisneros-Castillo, L.R., Oancea, A.D., Stüllen, C., et al.: A novel computer-assisted approach to evaluate multicellular tumor spheroid invasion assay. Scientific Reports **6**, 35099 (2016). https://doi.org/10.1038/srep35099
6. Cornelissen, F., Gustin, E., Cik, M.: Phaedra, a protocol-driven system for analysis and validation of high content imaging and flow cytometry. Journal of Biomedical Screening **17**(4), 496–506 (2012). https://doi.org/10.1177/1087057111432885
7. Hoarau-Véchot, J., Rafii, A., Touboul, C., et al.: Halfway between 2D and animal models: Are 3D cultures the ideal tool to study cancer-microenvironment interactions? International Journal of Molecular Sciences **19**(1), 181 (2018). https://doi.org/10.3390/ijms19010181
8. Hou, Y., Konen, J., Brat, D.J., et al.: Tasi: A software tool for spatial-temporal quantification of tumor spheroid dynamics. Scientific Reports **8**, 7248 (2018). https://doi.org/10.1038/s41598-018-25337-4
9. Ivanov, D.P., et al.: Multiplexing spheroid volume, resazurin and acid phosphatase viability assays for high-throughput screening of tumour spheroids and stem cell neurosphere. Plos One **9**(8), e103817 (2014). https://doi.org/10.1371/journal.pone.0103817
10. Kanopoulos, N., Vasanthavada, N., Baker, R.L.: Design of an image edge detection filter using the Sobel operator. IEEE Journal of Solid-State Circuits **23**(2), 358–367 (1988). https://doi.org/10.1109/4.996
11. Lv, D., Hu, Z., Lu, L., et al.: Three-dimensional cell culture: A powerful tool in tumor research and drug discovery (Review). Oncology Letters **14**(6), 6999–7010 (2017). https://doi.org/10.3892/ol.2017.7134
12. Moriconi, C., et al.: Insidia: A fiji macro delivering high-throughput and high-content spheroid invasion analysis. Biotechnology journal **12**(10), 1700140 (2017). https://doi.org/10.1002/biot.201700140
13. Nath, S., Devi, G.R.: Three-dimensional culture systems in cancer research: Focus on tumor spheroid model. Pharmacology & Therapeutics **163**, 94–108 (2016). https://doi.org/10.1016/j.pharmthera.2016.03.013
14. Otsu, N.: A threshold selection method from gray level histograms. IEEE Transaction on Systems, Man and Cybernetics **9**, 62–66 (1979). https://doi.org/10.1109/TSMC.1979.4310076
15. Piccinini, F.: Anasp: A software suite for automatic image analysis of multicellular spheroids. Computer Methods and Programs in Biomedicine **119**(1), 43–52 (2015). https://doi.org/10.1016/j.cmpb.2015.02.006

16. Piccinini, F., Tese, A., Zanoni, M.: Revims: Software tool for estimating the volumes of 3-d multicellular spheroids imaged using a light sheet fluorescence microscope. BioTechniques **63**(5), 227–229 (2017). https://doi.org/10.1177/1087057111432885
17. Ridler, T.W., Calvard, S.: Picture thresholding using an iterative selection method. IEEE Transaction on Systems, Man and Cybernetics **8**, 630–632 (1978). https://doi.org/10.1109/TSMC.1978.4310039
18. Rodenhizer, D., Dean, T., D'Arcangelo, E., et al.: The Current Landscape of 3D In Vitro Tumor Models: What Cancer Hallmarks Are Accessible for Drug Discovery? Advanced Healthcare Materials **7**(8), 1701174 (2018). https://doi.org/10.1002/adhm.201701174
19. Roerdink, J., Meijster, A.: The watershed transform: definitions, algorithms, and parallelization strategies. Fundamenta Informaticae **41**, 187–228 (2000). https://doi.org/10.3233/FI-2000-411207
20. Ronneberger, O., Fischer, P., Brox, T.: U-net: Convolutional networks for biomedical image segmentation. In: Medical Image Computing and Computer-Assisted Intervention – MICCAI 2015. Lecture Notes in Computer Science, vol. 9351, pp. 234–241 (2015). https://doi.org/10.1007/978-3-319-24574-4_28
21. Rueden, C.T., Schindelin, J., Hiner, M.C., et al.: Imagej2: Imagej for the next generation of scientific image data. BMC Bioinformatics **18**, 529 (2017). https://doi.org/10.1186/s12859-017-1934-z
22. Sadanandan, S.K., Karlsson, J., Wählby, C.: Spheroid segmentation using multiscale deep adversarial networks. In: 2017 IEEE International Conference on Computer Vision Workshops (ICCVW). pp. 36–41 (2017). https://doi.org/10.1109/ICCVW.2017.11
23. Vinci, M., Gowan, S., Boxall, F., et al.: Advances in establishment and analysis of three-dimensional tumor spheroid-based functional assays for target validation and drug evaluation. BMC Biology **10**, 29 (2012). https://doi.org/10.1186/1741-7007-10-29
24. World Health Organization: WHO report on cancer: setting priorities, investing wisely and providing care for all. World Health Organization (2020)